MULTI-STAGE PREDICTOR-CORRECTOR FLUXES FOR HYPERBOLIC EQUATIONS

E. F. Toro

Laboratory of Applied Mathematics
Faculty of Engineering, University of Trento
Trento, Italy
E-mail: toro@ing.unitn.it
Website: http://www.ing.unitn.it/toro

Abstract. In this paper we present a **MUlti-STAge** predictor-corrector approach, called **MUSTA**, for constructing upwind, monotone numerical fluxes to be used in numerical methods for solving hyperbolic conservation laws. The resulting methods achieve the accuracy of the best of upwind schemes, while retaining simplicity and generality. The schemes are accurate, robust and easy to implement and find their best justification when solving very complex systems for which the solution of the Riemann problem, in the classical sense, is too complex, too costly or is simply unavailable.

1 Introduction

When solving numerically non-linear systems of hyperbolic conservation laws via finite volume methods or discontinuous Galerkin finite element methods, there are essentially two approaches for providing a monotone numerical flux. The simplest approach utilises a symmetric stencil and does not explicitly make use of wave propagation information in the construction of the numerical flux. This approach gives rise to *centred* or *symmetric* schemes [16], [9], [14], [19], [41], [29], [18], [31], [1]. A more sophisticated approach utilises wave propagation information contained in the differential equations to construct the numerical flux. This is done through the exact or approximate solution of the Riemann problem. Due to the fact that wave propagation information is used, these methods are called *upwind* methods or *Godunov-type methods* [4], [8], [5], [38], [39], [22]. For up-to-date background on these methods see [17], [7], [15], [30], [36].

Generally, upwind methods are more accurate than centred methods. In fact, the Godunov first-order upwind method as applied to the model hyperbolic equation is the most accurate of all monotone first-order methods, in the sense that it has the smallest local truncation error; the scheme has numerical viscosity that is proportional to the wave speed. This means that the scheme resolves isolated stationary waves exactly, which is a distinguishing property of this class of numerical methods. Centred methods, on the other hand, have their largest numerical dissipation for the slowest waves, the stationary case being the worst situation, leading to large errors in the form of increasingly spreading of discontinuities as the solution is evolved in time. However, the better accuracy of upwind methods comes at a cost, the solution of the Riemann problem, a Cauchy problem for the governing equations with very special initial conditions consisting of two constant states separated by a discontinuity. The solution of the Riemann problem to be used in upwind methods may be the exact solution, if available, or an approximate solution. The quality of the global solution depends quite crucially on the particular Riemann solver user being used. There are linear and non-linear Riemann solvers available. Linear solvers tend to be simpler but suffer from a number of shortcomings, two of them being: they need an entropy fix and

they fail near low-density flows. Non-linear Riemann solvers are thus recommended. Then there are *complete* and *incomplete* Riemann solvers. Complete Riemann solvers may be approximate or exact and the structure of their representation of the solution includes all the wave families present in the exact solution of the Riemann problem. An incomplete Riemann solver on the other hand, does not include all wave families. An example of an incomplete Riemann solver is the popular HLL scheme [10], which only includes two wave families, those corresponding to the smallest and largest signal velocities and thus for a system of three or more equations intermediate waves are excluded. This results in unacceptable smearing of these waves, such as contact waves in the Euler equations of gas dynamics. As a consequence, the performance of upwind methods with incomplete Riemann solvers for *intermediate* waves is not superior to that of centred methods. For the faster waves the performance of upwind methods is very similar to that of good centred methods, with some advantage for upwind methods. The real difference in performance between centred and upwind methods is seen in resolving waves associated with linearly degenerate fields, for which upwind methods give much superior results. Centred or symmetric methods, although not as accurate as upwind methods, are much simpler to implement. This is a real asset for a numerical method, particularly for very complicated systems, for which the wave propagation information required by upwind methods is too difficult, too costly or simply impossible to obtain. The construction and implementation of centred methods is to a large extent, independent of the particular details of the system of conservation laws under consideration. Upwind methods on the other hand, are intimately linked to the particular set of equations, although the specific information provided by the equations is put to good use by upwind methods but the penalty is the lack of generality of the numerical method.

What is desirable, is an approach that has the accuracy of upwind methods and the simplicity and generality of centred methods, that is, an approach that applies equally well to any hyperbolic system. Such an approach would be ideally suited as a framework for developing numerical methods and software for complex industrial applications, with a long-term view. In this paper we present an approach that closely approximates the above aspirations. The computation of a numerical flux is carried out via a multi-stage predictor-corrector procedure, using a *simple* numerical flux at each stage. The most attractive approach to provide these simplified fluxes is the centred approach, but very simplified upwind intermediate fluxes are not excluded. In essence, our multi-stage approach may be regarded as an approximate Riemann solver in which the predictor stage *opens the Riemann fan* without making use of precise knowledge of the structure of the solution of the Riemann problem; in addition, the information extracted from the *opened* Riemann fan is precisely the information required for the evaluation of the intercell numerical flux sought. There is no logic associated with the complex solution-sampling procedure that is necessary when using an exact Riemann solver. The simpler logic of conventional approximate Riemann solvers when identifying the correct wave pattern is also absent in our approach. Our method finds its best justification for complex systems of conservation laws such as those in multi-phase fluid dynamics and magnetohydrodynamics. The flux can then be used as the building block for constructing schemes of higher order of accuracy following existing methodologies, such as TVD methods [10], [11], [20], [31]; ENO/WENO methods [13], [12], [26], [24], [25]; ADER methods [32], [34], [28], [23], [27] and discontinuous Galerkin finite element methods [2], [3], [37]. We remark that in higher-order schemes the difference in accuracy at the level of the first-order flux used, although less obvious, does persist, particularly for linearly degenerate fields and for long-time evolution problems [35].

The rest of this paper is organised as follows. In section 2 we review the Godunov method and well-known centred fluxes. In section 3 we present our multi-stage predictor-corrector approach. In section 4 we present some numerical results for the compressible Euler equations. Conclusions

are drawn in section 4.

2 Existing monotone schemes

We are interested in numerical schemes for solving hyperbolic partial differential equations in conservation-law form

$$\partial_t \mathbf{Q} + \partial_x \mathbf{F}\left(\mathbf{Q}\right) = \mathbf{0} \ , \tag{1}$$

in which $\mathbf{Q}$ is the vector of conserved variables and $\mathbf{F} = \mathbf{F}(\mathbf{Q})$ is the vector fluxes. In the presence of discontinuous solutions one uses the integral form of (1), which is obtained, for example, by integrating (1) on a control volume $[x_{i-\frac{1}{2}}, x_{i+\frac{1}{2}}] \times [t^n, t^{n+1}]$ in the x-t plane, leading to

$$\int_{x_{i-\frac{1}{2}}}^{x_{i+\frac{1}{2}}} \mathbf{Q}(x,t^{n+1})dx = \int_{x_{i-\frac{1}{2}}}^{x_{i+\frac{1}{2}}} \mathbf{Q}(x,t^{n})dx - \left[\int_{t^n}^{t^{n+1}} \mathbf{F}\left(\mathbf{Q}(x_{i+\frac{1}{2}},t)\right) dt - \int_{t^n}^{t^{n+1}} \mathbf{F}\left(\mathbf{Q}(x_{i-\frac{1}{2}},t)\right) dt \right] \ , \tag{2}$$

from which we obtain

$$\mathbf{Q}_i^{n+1} = \mathbf{Q}_i^n - \frac{\Delta t}{\Delta x}\left[\mathbf{F}_{i+\frac{1}{2}} - \mathbf{F}_{i-\frac{1}{2}}\right] \ , \tag{3}$$

where

$$\mathbf{Q}_i^n = \frac{1}{\Delta x}\int_{x_{i-\frac{1}{2}}}^{x_{i+\frac{1}{2}}} \mathbf{Q}(x,t^n)dx \ , \ \ \mathbf{F}_{i+\frac{1}{2}} = \frac{1}{\Delta t}\int_{t^n}^{t^{n+1}} \mathbf{F}(\mathbf{Q}(x_{i+\frac{1}{2}},t))dt \ . \tag{4}$$

We can construct numerical methods based on the control volume formula (3) by finding numerical fluxes that are approximations to the time-integral average of the fluxes at the control volume boundaries, given in (4). The numerical scheme will then evolve in time integral averages in control volumes. Next we briefly review two classical ways of defining a numerical flux.

2.1 The Riemann problem and the Godunov flux

Godunov's method [8] defines the numerical flux $\mathbf{F}_{i+\frac{1}{2}}$ in terms of the solution of the Riemann problem, which is the initial value problem for (1) subject to the special initial conditions

$$\mathbf{Q}(x,0) = \begin{cases} \mathbf{Q}_i^n & \text{if} \quad x < x_{i+\frac{1}{2}} \ , \\ \mathbf{Q}_{i+1}^n & \text{if} \quad x > x_{i+\frac{1}{2}} \ . \end{cases} \tag{5}$$

Fig. 1 shows the structure of the solution of the Riemann problem in the x-t plane for an $m \times m$ non-linear system. The so so called *Riemann fun* consists of $m+1$ constant states separated by m wave families, each one associated with the real eigenvalue $\lambda^{(k)}$. The similarity solution of (1), (5) depends of the ratio x/t and is denoted by $\mathbf{Q}_{i+\frac{1}{2}}(x/t)$. The Godunov intercell numerical flux is found by first evaluating $\mathbf{Q}_{i+\frac{1}{2}}(x/t)$ at $x/t = 0$, that is along the t-axis in Fig. 1, and then evaluating the physical flux vector $\mathbf{F}(\mathbf{Q})$ in (1) at $\mathbf{Q}_{i+\frac{1}{2}}(0)$, namely

$$\mathbf{F}_{i+\frac{1}{2}}^{God} = \mathbf{F}(\mathbf{Q}_{i+\frac{1}{2}}(0)) \ . \tag{6}$$

The exact solution will invariably involve at least one iterative procedure and thus in practice, whenever possible, one uses approximate Riemann solvers. For a review on Riemann solvers the reader is referred to [30].

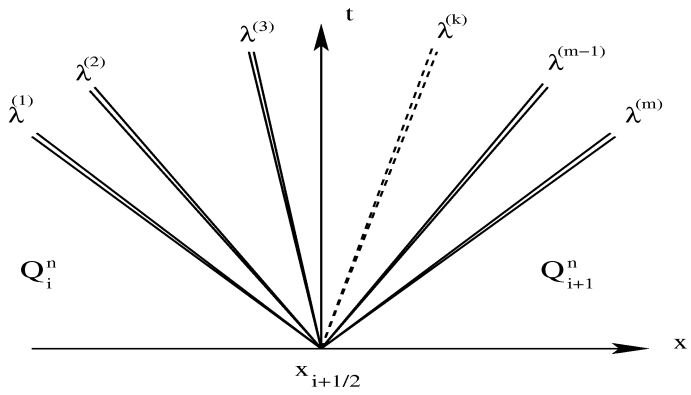

Figure 1: Structure of the solution of the Riemann problem for an $m \times m$ hyperbolic system.

2.2 Centred fluxes

We briefly review intercell numerical fluxes of the centred type to be used directly into the conservative formula (3). Unlike upwind methods, centred fluxes do not make use of the solution of the Riemann problem and generally they can be computed explicitly as functions of the initial data, namely

$$\mathbf{F}_{i+\frac{1}{2}} = \mathbf{F}_{i+\frac{1}{2}}(\mathbf{Q}_i^n, \mathbf{Q}_{i+1}^n) \; . \tag{7}$$

One may interpret centred fluxes as resulting from a low-level approximation to the solution of the Riemann problem, in which the Riemann fun *is not opened* to extract the appropriate value of the solution for flux evaluation.

Two classical centred fluxes are the Lax-Friedrichs flux

$$\mathbf{F}_{i+\frac{1}{2}}^{LF} = \mathbf{F}_{i+\frac{1}{2}}^{LF}(\mathbf{Q}_i^n, \mathbf{Q}_{i+1}^n) = \frac{1}{2}[\mathbf{F}(\mathbf{Q}_i^n) + \mathbf{F}(\mathbf{Q}_{i+1}^n)] - \frac{1}{2}\frac{\Delta x}{\Delta t}[\mathbf{Q}_{i+1}^n - \mathbf{Q}_i^n] \tag{8}$$

and the two-step Lax-Wendroff flux

$$\left.\begin{array}{l} \mathbf{F}_{i+\frac{1}{2}}^{LW} = \mathbf{F}(\mathbf{Q}_{i+\frac{1}{2}}^{n+\frac{1}{2}}) \; , \\ \mathbf{Q}_{i+\frac{1}{2}}^{n+\frac{1}{2}} = \frac{1}{2}[\mathbf{Q}_i^n + \mathbf{Q}_{i+1}^n] - \frac{1}{2}\frac{\Delta t}{\Delta x}[\mathbf{F}(\mathbf{Q}_{i+1}^n) - \mathbf{F}(\mathbf{Q}_i^n)] \; . \end{array}\right\} \tag{9}$$

Another, more recent, centred flux is the FORCE flux [29], [30], [31], [1]. This was derived from a deterministic interpretation of the staggered-grid version of Glimm's method [6] and results in a non-staggered one-step conservative scheme of the form (3) with intercell numerical flux given by

$$\mathbf{F}_{i+\frac{1}{2}}^{\text{force}} = \mathbf{F}_{i+\frac{1}{2}}^{\text{force}}(\mathbf{Q}_i^n, \mathbf{Q}_{i+1}^n) = \frac{1}{4}\left[\mathbf{F}(\mathbf{Q}_i^n) + 2\mathbf{F}(\mathbf{Q}_{i+\frac{1}{2}}^{n+\frac{1}{2}}) + \mathbf{F}(\mathbf{Q}_{i+1}^n) - \frac{\Delta x}{\Delta t}\left(\mathbf{Q}_{i+1}^n - \mathbf{Q}_i^n\right)\right] \; , \tag{10}$$

with $\mathbf{Q}_{i+\frac{1}{2}}^{n+\frac{1}{2}}$ as in (9). A surprising outcome is that the intercell flux (10) is in fact the arithmetic mean of the Lax-Wendroff flux $\mathbf{F}_{i+\frac{1}{2}}^{LW}$ and the Lax-Friedrichs flux $\mathbf{F}_{i+\frac{1}{2}}^{LF}$. More insight is given by considering the model hyperbolic equation (18). Fig. 2 shows a plot containing the family of three-point schemes that can be written as a convex average of $\mathbf{F}_{i+\frac{1}{2}}^{LF}$ (bottom boundary) and $\mathbf{F}_{i+\frac{1}{2}}^{LW}$ (top boundary), in which the *FORCE* flux (10) corresponds to the value $\omega = 1/2$. Larger values of the weight ω correspond to schemes with smaller numerical dissipation. The whole

region is subdivided into a bottom region of monotone schemes, for $\omega \leq \omega_g \equiv \frac{1}{1+c}$, and an upper region of non-monotone schemes, for which $\omega > \omega_g$. The line $\omega = \frac{1}{1+c}$ corresponds precisely to the Godunov first-order upwind scheme, which is the scheme with the smallest numerical dissipation and monotone. Here c is the Courant number. Also shown there is the weight for the Godunov first-order centred method [9], which is linearly stable for $0 \leq c \leq \frac{1}{2}\sqrt{2}$, but is not monotone in the range $0 \leq c \leq \frac{1}{2}$. If we were to select an average with constant weight ω (independent of wave propagation information), then the scheme with the smallest numerical dissipation would be the *FORCE* scheme. In [1] it is shown that the conservative scheme (3) with the FORCE flux (10) is convergent for a 2×2 non-linear system of conservation laws.

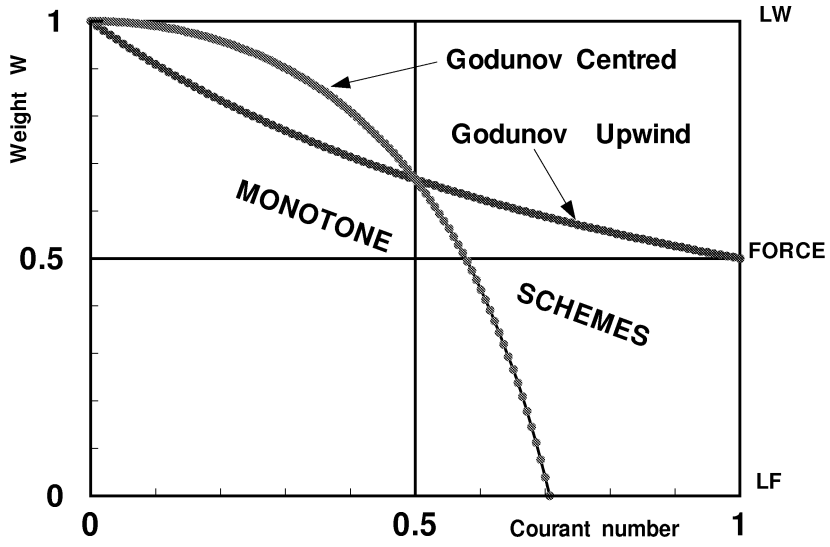

Figure 2: Family of three-point schemes as convex average of the Lax-Friedrichs (bottom) and Lax-Wendroff (top) methods.

3 The MUSTA approach

We propose to construct a numerical flux based on a multi-stage predictor-corrector approach. In the predictor step we propose to use a simple and robust numerical flux to *open the Riemann fun* and extract the relevant information for the corrector step, which involves the final intercell flux evaluation. The expectation is that the resulting flux arising from the *opened fun* will be close, in some sense, to the Godunov flux. The motivation behind is to obtain a simple (possibly centred) numerical flux that is applicable to any system of conservation laws and that is a good approximation to the best first-order method, namely the first-order upwind method of Godunov. Given two constant states $\mathbf{Q}_i^n$ and $\mathbf{Q}_{i+1}^n$ separated by a discontinuity at $x_{i+\frac{1}{2}}$ the Godunov method solves the corresponding Riemann problem (1), (5) to find a solution $\mathbf{Q}_{i+\frac{1}{2}}(x/t)$, with the Godunov flux obtained by evaluating the flux function at the solution of the local Riemann problem at $x/t = 0$, as given by (6). Generally, the optimal accuracy achieved by the Godunov method results from *opening the Riemann fun*, see Fig. 1. On the other hand, centred methods, do not do this and just use the initial data on the left and right sides of the initial discontinuity, see (8) for example, to compute a numerical flux.

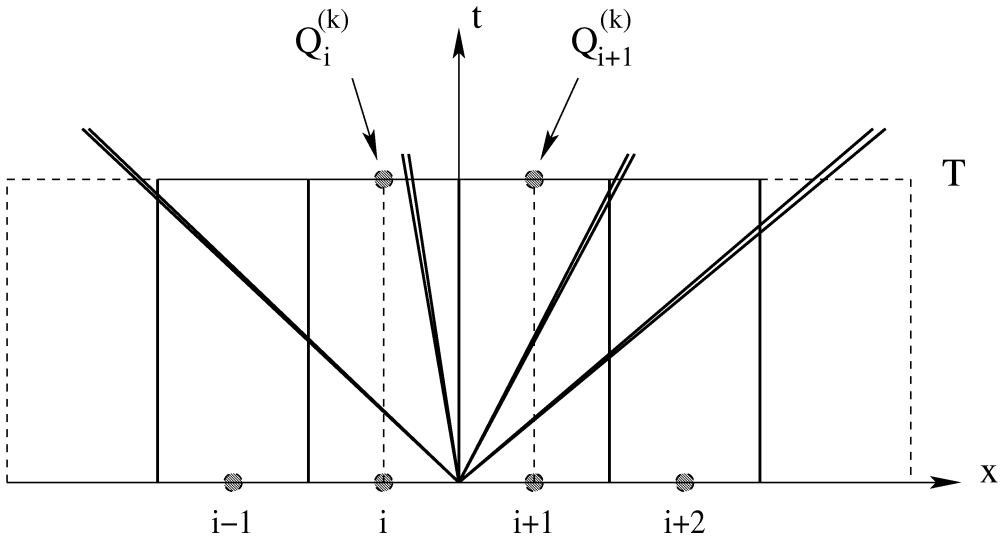

Figure 3: Illustration of the multi-stage procedure for a 4×4 system.

3.1 Opening the Riemann fan

The task at hand is to compute a numerical flux at the interface $x = x_{i+\frac{1}{2}}$ separating control volumes with averages $\mathbf{Q}_i^n$ (left) and $\mathbf{Q}_i^n$ (right); see Figs. 1 and 3. Suppose that we *open the Riemann fun* by solving the corresponding Riemann problem numerically on a mesh of r cells to the left of $x_{i+\frac{1}{2}}$ and r cells to the right of $x_{i+\frac{1}{2}}$ using a given numerical method, probably centred and monotone. The sought numerical solution is that for large time T. At every time step l we have the discrete sets of values $\mathbf{Q}_{i-r+j}^{(l)}, j = 1, \ldots, r$ and $\mathbf{Q}_{i+j}^{(l)}, j = 1, \ldots, r$. The initial conditions for such numerical problem would be $\mathbf{Q}_{i-r+j}^{(1)} = \mathbf{Q}_i^n, j = 1, \ldots, r$ and $\mathbf{Q}_{i+j}^{(1)} = \mathbf{Q}_{i+1}^n, j = 1, \ldots, r$. The two vectors of interest at the l-stage are those adjacent to the interface, namely $\mathbf{Q}_i^{(l)}$ and $\mathbf{Q}_{i+1}^{(l)}$. Fig. 3 illustrates the situation for $r = 2$. The computational domain requires the application of boundary conditions, which are implemented by adding two extra fictitious or ghost cells on the left and right of the domain. We apply transmissive boundary conditions so as to allow the passage of waves emerging from $x = x_{i+\frac{1}{2}}$ through the numerical boundaries. If

$$|\mathbf{Q}_j^{(l+1)} - \mathbf{Q}_j^{(l)}| < \epsilon \ , \quad \text{for} \ \ j = i, i+1 \ , \tag{11}$$

where $||$ is a suitable norm and $\epsilon > 0$ is a small tolerance, we stop the time-marching procedure. The two vectors of interest for the corrector (final) step k are $\mathbf{Q}_i^{(k)}$ and $\mathbf{Q}_{i+1}^{(k)}$. In the case of Godunov's method one solves the Riemann problem and finds a single value *at the interface* $x = x_{i+\frac{1}{2}}$. In our method we still have two values either side of the interface. It is likely that these two values are close and in the exact solution for large time these are probably identical. It can also happen that these two values are separated by one of the waves in the solution of the Riemann problem, in which case these two vectors will be different. Examples of this second case arise when the Riemann problem solution contains a stationary discontinuity or a transonic rarefaction. In our approach the existing discontinuity between $\mathbf{Q}_i^{(k)}$ and $\mathbf{Q}_{i+1}^{(k)}$ is resolved in the corrector step by a simple flux, such as a centred flux that requires two arguments, namely

$$\mathbf{F}_{i+\frac{1}{2}}^{(k)} = \mathbf{F}_{i+\frac{1}{2}}^{(k)}(\mathbf{Q}_i^{(k)}, \mathbf{Q}_{i+1}^{(k)}) \ , \tag{12}$$

where $\mathbf{F}_{i+\frac{1}{2}}$ is any suitably simple numerical flux. The suggested procedure is expected to produce a numerical flux very close to that of the upwind method of Godunov, the optimal scheme. This is certainly the case if the interface position is straddled by a constant state or a rarefaction wave. There is no doubt that the suggested numerical procedure for solving the Riemann problem and evaluating a numerical flux is very simple and could be widely applicable, in principle, to any system of conservation laws, complicated or not, and all of this without making use of any knowledge of the equations, such as its eigenstructure. However, the obvious objection to the approach, as presented so far, is its computational cost. There are two factors that determine the cost of the above procedure, namely the mesh used ($2r$) and the stopping criterion in (11), or equivalently, the number of stages in the predictor step. We have performed numerical experiments for large r and k and found that the resulting scheme approaches the result of the Godunov upwind method used in conjunction with the exact Riemann solver. More importantly, we have also found that even for small values of r and k one can obtain solutions that are sufficiently accurate for the purpose of flux evaluation.

The simplest scheme, and the one we propose for practical use, takes $r = 1$ and k small. Defining $\mathbf{Q}_i^{(1)} \equiv \mathbf{Q}_i^n$ and $\mathbf{Q}_{i+1}^{(1)} \equiv \mathbf{Q}_{i+1}^n$ the multi-stage predictor step is

$$\left.\begin{aligned} \mathbf{Q}_i^{(l+1)} &= \mathbf{Q}_i^{(k)} - \tfrac{\Delta t}{\Delta x}[\mathbf{F}_{i+\frac{1}{2}}^{(l)} - \mathbf{F}(\mathbf{Q}_i^{(l)})] \\ \mathbf{Q}_{i+1}^{(l+1)} &= \mathbf{Q}_{i+1}^{(l)} - \tfrac{\Delta t}{\Delta x}[\mathbf{F}(\mathbf{Q}_{i+1}^{(l)}) - \mathbf{F}_{i+\frac{1}{2}}^{(l)}] \end{aligned}\right\} \tag{13}$$

The corrector step is of the form (12). Note that we are not restricted to use the same flux in the predictor and the corrector steps. It is easy to verify that the numerical flux resulting from the corrector step is *consistent* if the fluxes employed in both the predictor and corrector steps are consitent. That is, for $\mathbf{Q}_i^n = \mathbf{Q}_{i+1}^n = \bar{\mathbf{Q}}$ we have

$$\mathbf{F}_{i+\frac{1}{2}} = \mathbf{F}_{i+\frac{1}{2}}(\mathbf{Q}_i^n, \mathbf{Q}_{i+1}^n) = \mathbf{F}_{i+\frac{1}{2}}(\bar{\mathbf{Q}}, \bar{\mathbf{Q}}) = \mathbf{F}(\bar{\mathbf{Q}}) \; .$$

The multi-stage predictor step is by no means restricted to conservative-type schemes. Note that actual flux is that given by (12). The states $\mathbf{Q}_i^{(k)}, \mathbf{Q}_{i+1}^{(k)}$ may be found by other procedures. For example we may write the governing equations (1) in non-conservative form

$$\partial_t \mathbf{W} + \mathbf{A}\,(\mathbf{W})\,\partial_x \mathbf{Q} = \mathbf{0} \; , \tag{14}$$

where $\mathbf{W}$ is a vector of suitably chosen variables; they could also be the conservative variables. A corresponding multi-stage predictor step is

$$\left.\begin{aligned} \mathbf{W}_i^{(l+1)} &= \mathbf{W}_i^{(l)} - \tfrac{\Delta t}{\Delta x}\mathbf{A}_i^{(l)}[\mathbf{W}_{i+\frac{1}{2}}^{(l)} - \mathbf{W}_i^{(l)})] \\ \mathbf{W}_{i+1}^{(l+1)} &= \mathbf{W}_{i+1}^{(l)} - \tfrac{\Delta t}{\Delta x}\mathbf{A}_{i+1}^{(l)}[\mathbf{W}_{i+1}^{(l)} - \mathbf{W}_{i+\frac{1}{2}}^{(l)})] \end{aligned}\right\} \tag{15}$$

Here $\mathbf{W}_{i+\frac{1}{2}}^{(l)}$ is a suitable *intermediate* vector; see Toro and Siviglia [35] for possible choices for intermediate vectors arising from non-conservative centred schemes. The coefficient matrices are

$$\mathbf{A}_i^{(l)} = \mathbf{A}(\mathbf{W}_i^{(l)}) \; , \quad \mathbf{A}_{i+1}^{(l)} = \mathbf{A}(\mathbf{W}_{i+1}^{(l)}) \; .$$

3.2 The 2-stage $FORCE^2$ flux

In this section we study the particular scheme in which the $FORCE$ flux (10) is used as the basic flux in both the predictor step (13) and the corrector step (12). More particularly, we study a two-stage predictor corrector scheme. Denoting by $\mathbf{Q}_i^{(1)} = \mathbf{Q}_i^n$ and $\mathbf{Q}_{i+1}^{(1)} = \mathbf{Q}_{i+1}^n$ the predictor step is

$$\left.\begin{aligned} \mathbf{Q}_i^{(2)} &= \mathbf{Q}_i^{(1)} - \alpha\tfrac{\Delta t}{\Delta x}[\mathbf{F}_{i+\frac{1}{2}}^{(force)}(\mathbf{Q}_i^{(1)}, \mathbf{Q}_{i+1}^{(1)}) - \mathbf{F}(\mathbf{Q}_i^n)] \\ \mathbf{Q}_{i+1}^{(2)} &= \mathbf{Q}_{i+1}^{(1)} - \alpha\tfrac{\Delta t}{\Delta x}[\mathbf{F}(\mathbf{Q}_{i+1}^n) - \mathbf{F}_{i+\frac{1}{2}}^{(force)}(\mathbf{Q}_i^{(1)}, \mathbf{Q}_{i+1}^{(1)})] \end{aligned}\right\} \tag{16}$$

and the corrector step is

$$\mathbf{F}_{i+\frac{1}{2}}^{force^2} = \mathbf{F}_{i+\frac{1}{2}}^{(force)}(\mathbf{Q}_i^{(2)}, \mathbf{Q}_{i+1}^{(2)}) \, . \tag{17}$$

The parameter α determines the size of the time step in the predictor stage and we keep it as free parameter to enforce monotonicity, for example. We shall determine the useful values of α by studying the scheme as applied to the model linear advection equation with constant coefficient λ,

$$\partial_t q + \lambda \partial_x q = 0 \, . \tag{18}$$

The Godunov upwind flux is

$$\left.\begin{aligned} f_{i+\frac{1}{2}}^{God} &= \beta_L(\lambda q_i^n) + \beta_R(\lambda q_{i+1}^n) \\ \beta_L &= \tfrac{1}{2}(1 + sign(c)) \, , \quad \beta_R = \tfrac{1}{2}(1 - sign(c)) \end{aligned}\right\} \tag{19}$$

where $c = \frac{\lambda \Delta t}{\Delta x}$ is the Courant, or CFL, number.

As already stated, the first-order upwind scheme of Godunov is the optimal scheme in the class of first-order monotone schemes. The coefficient of the leading term of the local truncation error is $C_{god} = \frac{1}{2}\Delta x \lambda(1 - |c|)$. Obviously C_{god} tends to zero as the mesh size Δx tends to zero, but the distinguishing feature is that it is zero when the speed of wave propagation λ is zero, giving upwind schemes the unique property of recognising exactly isolated *stationary* waves. It is precisely for this type of waves that any other method will have difficulties with, as is well known. It is then justified to compare other fluxes with the optimal flux (19).

The Lax-Friedrichs flux is

$$\left.\begin{aligned} f_{i+\frac{1}{2}}^{LF} &= \beta_L(\lambda q_i^n) + \beta_R \lambda q_{i+1}^n) \\ \beta_L &= \tfrac{(c+1)}{2c} \, , \quad \beta_R = \tfrac{(c-1)}{2c} \end{aligned}\right\} \tag{20}$$

The $FORCE^1$ flux is

$$\left.\begin{aligned} f_{i+\frac{1}{2}}^{force} &= \beta_L(\lambda q_i^n) + \beta_R \lambda q_{i+1}^n) \\ \beta_L &= \tfrac{(1+c)^2}{4c} \, , \quad \beta_R = -\tfrac{(1-c)^2}{4c} \end{aligned}\right\} \tag{21}$$

The 2-stage $FORCE^2$ flux is

$$\left.\begin{aligned} f_{i+\frac{1}{2}}^{force^2} &= f_{i+\frac{1}{2}}^{force^2}(q_i^n, q_{i+1}^n) = \beta_L(\lambda q_i^n) + \beta_R(\lambda q_{i+1}^n) \\ \beta_L &= \tfrac{1}{16c}\left\{(c+1)^2[4 - (\alpha c - 1)^2] - (c-1)^2(\alpha c + 1)^2\right\} \\ \beta_R &= \tfrac{1}{16c}\left\{(c+1)^2(\alpha c - 1)^2 - (c-1)^2[4 - (\alpha c + 1)^2]\right\} \end{aligned}\right\} \tag{22}$$

We now determine conditions on the free parameter α in (16), (22) through the model equation (18). A desirable property for the flux to satisfy is *monotonicity*. Recall that a flux $f_{i+\frac{1}{2}}(q_L, q_R)$ is said to be monotone if it is an increasing function of its first argument and a decreasing function of its second argument, that is

$$\frac{\partial}{\partial q_L} f_{i+\frac{1}{2}}(q_L, q_R) \geq 0 \;\text{ and }\; \frac{\partial}{\partial q_R} f_{i+\frac{1}{2}}(q_L, q_R) \leq 0 \,. \tag{23}$$

Clearly the Lax-Friedrichs and $FORCE^1$ fluxes are monotone, as $\beta_L \geq 0$ and $\beta_R \leq 0$. For the $FORCE^2$ flux, monotonicity depends on the parameter α, for which we need to satisfy conditions (23). That is we must satisfy

$$\beta_L = \frac{1}{16c}\left\{(c+1)^2[4-(\alpha c-1)^2] - (c-1)^2(\alpha c+1)^2\right\} \geq 0 \tag{24}$$

and

$$\beta_R = \frac{1}{16c}\left\{(c+1)^2(\alpha c-1)^2 - (c-1)^2[4-(\alpha c+1)^2]\right\} \leq 0 \,. \tag{25}$$

Algebraic manipulations of inequality (24) show that a sufficient condition for its satisfaction is $\alpha \leq \alpha_g \equiv \frac{1}{c}$. The upper bound $\alpha_g \equiv \frac{1}{c}$ is significant, as when $\alpha = \alpha_g = \frac{1}{c}$ and $c > 0$, $\beta_L = 1$ and $\beta_R = 0$, giving the flux for the Godunov first-order scheme (19). A good choice that is independent of c is $\alpha = 1$.

Concerning the second monotonicity condition (25) we first look for the limiting case $\beta_R = 0$. We obtain a quadratic for α with two solutions, namely

$$\alpha_b(c) = -\frac{c^2 - 4c + 1}{c(c^2+1)} \quad \text{and} \quad \alpha_g(c) = \frac{1}{c} \,. \tag{26}$$

These solutions are displayed in Fig. 4 as functions of the Courant number c. Note that $\alpha_b(c) \leq \alpha_g(c)$ and we search for choices of α satisfying

$$\alpha_b(c) \leq \alpha \leq \alpha_g(c) \,. \tag{27}$$

It is desirable to find solutions for α that are independent of wave propagation information, that is, independent of c. Thus we look for a constant value of α, let us call it α_0 that is consistent with monotonicity and with the largest possible value of the Courant number used to enforce the stability condition of the scheme. From Fig. 4 we see that the line $\alpha = \alpha_0$ must be tangent to $\alpha_b(c)$ at some c, with $0 < c < 1$, and being above $\alpha_b(c)$ satisfies one monotonicity constraint. However, this line $\alpha = \alpha_0$ will intersect the upper bound $\alpha_g(c)$ at some c_0, with $0 < c_0 < 1$. For $c > c_0$ monotonicity will be lost. By numerically solving the corresponding non-linear equations we find that

$$\alpha_0 = 1.276447 \;\text{ and }\; c_0 = 0.7834249 \,. \tag{28}$$

It is found that the line $\alpha = \alpha_0$ is tangent to $\alpha_b(c)$ at $c = 0.6217106$ and intersects $\alpha_g(c)$ at the largest possible CFL number consistent with monotonicity at $c_0 = 0.7834249$. Use of CFL numbers greater than c_0 means loosing monotonicity, as we exceed the limiting value $\alpha_g(c)$ that corresponds to the Godunov first-order upwind method. For smooth solutions this will result in smaller numerical dissipation than for the Godunov method, but for discontinuities it means producing spurious oscillations.

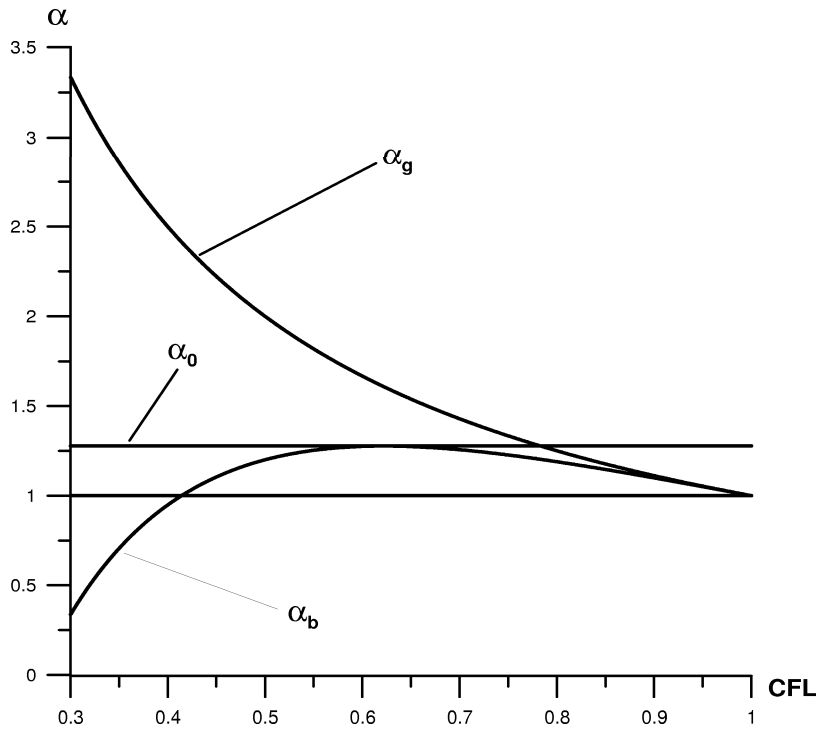

Figure 4: Monotonicity condition for coefficient β_R results in monotonicity region in the α-c plane, which lies between the top curve α_g, which corresponds to the Godunov's upwind scheme, and the bottom curve α_b.

Numerical experiments for the linear advection equation (18) for discontinuous initial conditions confirm the theoretical findings. We also observe that for Courant numbers $c_0 < c < c_{emp} \approx 0.95$ oscillations are hardly visible and are smoothed out as time evolves. For larger CFL numbers oscillations are unacceptable. For non-linear systems we find that the scheme can be used with with practical choices of CFL numbers of about 0.90, which is what is normally used for schemes with linear stability condition of $|c| \leq 1$.

A second way of trying to enforce monotonicity is to first select the optimal value of α, independent of c, that will satisfy condition (24). This value is $\alpha = 1$. Use of this in the coefficient β_R in (25) gives a range of CFL numbers for which $\beta_R > 0$ and in which monotonicity is lost. Fig. 5 shows the behaviour of the coefficients β_L and β_R for $\alpha = 1$, for Courant numbers c, with $0 < c \leq 1$. It is seen that the loss of monotonicity is very slight, the coefficient β_R is just above 0 for the range of CFL numbers $\sqrt{2} - 1 < c \leq 1$. The maximum of β_R occurs for $c = 0.5773503$ and is $\beta_{R,max} = 0.0188$, which is close to zero. This loss of monotonicity takes place for intermediate wave speeds and dissapears as c tends to 1. Therefore, for practical computations we recommend using $\alpha = 1$ in the $FORCE^2$ scheme (13), (12).

We have also calculated the flux error of a given flux $f^{(x)}_{i+\frac{1}{2}}(q^n_i, q^n_{i+1})$ as compared with the best first-order monotone scheme, the Godunov first-order upwind scheme, namely

$$E_x = |f^{(x)}_{i+\frac{1}{2}}(q^n_i, q^n_{i+1}) - f^{God}_{i+\frac{1}{2}}(q^n_i, q^n_{i+1})| \, . \tag{29}$$

We have considered the case $\lambda > 0$ and Table 1 shows the results, normalised by $\lambda|q^n_{i+1} - q^n_{i+1}|$. As expected, errors are largest as c tends to zero and the least accurate flux is that of Lax-Friedrichs, with $FORCE^1$ giving better results, which are again improved by the 2-stage $FORCE^2$ scheme.

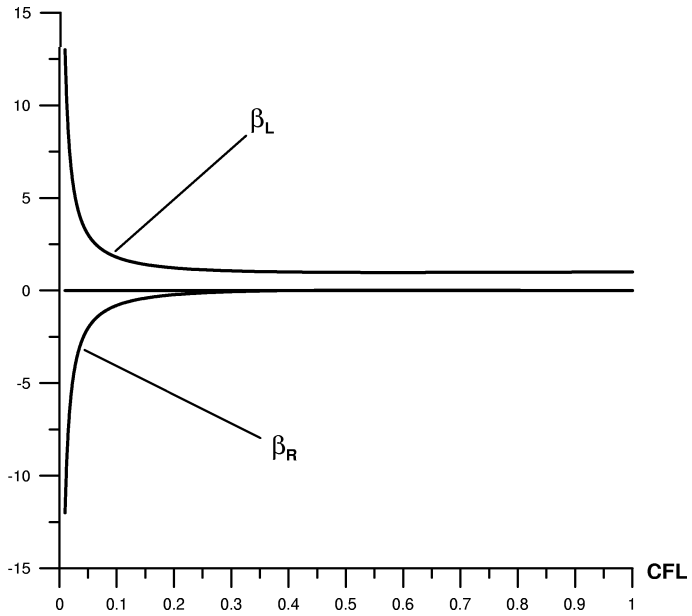

Figure 5: Variation of the coefficients β_L and β_R for the $FORCE^2$ for the linear advection equation, as functions of the CFL number c for $\alpha = 1.0$.

Flux	Error
Lax-Friedrichs	$\frac{1-c}{2c}$
$FORCE^1$	$\frac{1}{2}(1-c) \times \frac{1-c}{2c}$
$FORCE^2$	$\frac{(c+1)^2(\alpha c-1)^2+(c-1)^2(\alpha c+1)^2-4(c-1)^2}{8(1-c)} \times \frac{1-c}{2c}$

Table 1. Normalised flux errors the Lax-Friedrichs, $FORCE^1$ and $FORCE^2$ fluxes as applied to the linear advection equation with $\lambda > 0$.

Empirically, we have found that by increasing the number of stages in the predictor step the accuracy of the scheme tends to that of the model scheme, the Godunov first-order upwind method.

3.3 Other schemes

The numerical flux in the predictor step (13) does not need be the same as that in the corrector step (12). For example, one could use the Lax-Friedrichs flux (8) for the predictor (13) and the $FORCE$ flux (10) in the final flux evaluation. Another possibility is to use the Lax-Wendroff flux (9) in the predictor and the corrector steps. It is well-known that the Lax-Wendroff flux, if used as a single-stage scheme, is oscillatory. We have carried out some analysis for the two-stage Lax-Wendroff scheme as applied to the model equation (18). The corrector 2-stage Lax-Wendroff type flux is

$$f^{(2)}_{i+\frac{1}{2}} = \beta_L(\lambda q^n_i) + \beta_R(\lambda q^n_{i+1}) \,, \tag{30}$$

with coefficients given by

$$\left.\begin{aligned} \beta_L &= \tfrac{1}{2}(1+c) + \tfrac{1}{4}(1+c)(1-\alpha c)\alpha c + \tfrac{1}{4}(1-c)(1+\alpha c)\alpha c \\ \beta_R &= \tfrac{1}{2}(1-c) - \tfrac{1}{4}(1+c)(1-\alpha c)\alpha c - \tfrac{1}{4}(1-c)(1+\alpha c)\alpha c \end{aligned}\right\} \tag{31}$$

In the predictor step we have advanced the solution by a time $\alpha\Delta t$, where Δt is a stable time step for the overall scheme. In the corrector step we have evaluated the Lax-Wendroff flux, as for a time step Δt. The free parameter α will be used to enforce monotonicity, for which we require $\beta_L \geq 0$ and $\beta_R \leq 0$. The first condition is met for all values of α and CFL numbers c in the interval $[0, 1]$. The second condition cannot be met without choosing α as a function of the CFL number, an undesirable, or unwanted condition, as we would not want to resort to any form of upwinding, for which we would need information on wave propagation. We note however that $\beta_R = 0$ gives two choices for α, namely

$$\alpha_B = \frac{1 - \sqrt{4c(c-1)+1}}{2c^2} \quad , \quad \alpha_T = \frac{1 + \sqrt{4c(c-1)+1}}{2c^2} \, . \tag{32}$$

We note that $\beta_R \leq 0$ for $\alpha_M = \frac{1}{2}(\alpha_B + \alpha_T) = \frac{1}{2c^2}$. All three curves α_B, α_M and α_T cross over at $c = 1/2$. For systems this condition could be implemented as follows. Given a range of waves and corresponding CFL numbers $\{c_k\}$ we could choose $\alpha = max_k \{\alpha_B(c_k), \alpha_T(c_k)\}$. It seems as if schemes based on the Lax-Wendroff flux are not useful. This is supported by numerical experiments, which show that the schemes are oscillatory for the range of smaller CFL numbers. We have also analysed 2-stage schemes based on other fluxes, such as the Godunov centred flux, with similarly dissapointing results. However, we believe that there is still room for more investigations in this area. In the next section we give a detailed algorithm for a successful multi-stage scheme.

3.4 Algorithm for the k-stage $FORCE^k$ scheme

Here we propose a **MUSTA**-type scheme that can be used in practice. It is based on applying the $FORCE$ flux (10) for both the multi-stage predictor (13) and the corrector (12). It is a generalisation of the 2-stage $FORCE^2$ scheme analysed in section 3.2. The scheme has essentially two stages and is started by setting $l = 1$, $\mathbf{Q}_i^{(1)} = \mathbf{Q}_i^n$ and $\mathbf{Q}_{i+1}^{(1)} = \mathbf{Q}_{i+1}^n$. Then we do:

1. Flux evaluation:

$$\mathbf{F}_i^{(l)} = \mathbf{F}(\mathbf{Q}_i^{(l)}) \, , \quad \mathbf{F}_{i+1}^{(l)} = \mathbf{F}(\mathbf{Q}_{i+1}^{(l)}) \, ,$$

$$\mathbf{Q}_{i+\frac{1}{2}}^{(l)} = \frac{1}{2}[\mathbf{Q}_i^{(l)} + \mathbf{Q}_{i+1}^{(l)}] - \frac{1}{2}\frac{\Delta t}{\Delta x}[\mathbf{F}_{i+1}^{(l)} - \mathbf{F}_i^{(l)}] \, , \quad \mathbf{F}_M^{(l)} = \mathbf{F}(\mathbf{Q}_{i+\frac{1}{2}}^{(l)}) \, ,$$

$$\mathbf{F}_{i+\frac{1}{2}}^{(l)} = \frac{1}{4}\left[\mathbf{F}_i^{(l)} + 2\mathbf{F}_M^{(l)} + \mathbf{F}_{i+1}^{(l)} - \frac{\Delta x}{\Delta t}\left(\mathbf{Q}_{i+1}^{(l)} - \mathbf{Q}_i^{(l)}\right)\right] \, .$$

2. Open Riemann fan:

$$\mathbf{Q}_i^{(l+1)} = \mathbf{Q}_i^{(l)} - \frac{\Delta t}{\Delta x}[\mathbf{F}_{i+\frac{1}{2}}^{(l)} - \mathbf{F}_i^{(l)}] \, , \quad \mathbf{Q}_{i+1}^{(l+1)} = \mathbf{Q}_{i+1}^{(l)} - \frac{\Delta t}{\Delta x}[\mathbf{F}_{i+1}^{(l)} - \mathbf{F}_{i+\frac{1}{2}}^{(l)}] \, .$$

3. Goto step 1

The procedure is stopped at the end of Step 1 if the desired number of stages k has been reached.

From examining the algorithm for the k-stage $FORCE^k$ scheme we see that the number of elementary arithmetic operations needed for evaluation of the intercell numerical flux is roughly k(3 flux evaluations $+11m + 8) - 4m - 2$, where k is the number of stages in the predictor and m is the number of equations. There are no fractional powers involved, unless they are present at the level of the equation of state, for example, via the flux evaluations in Step 1. For the

one-dimensional Euler equations ($m = 3$), a 2-stage scheme requires 68 operations and three flux evaluations. This is comparable to typical existing approximate Riemann solvers, such as Roe's solver [22] or the HLLC solver [33], for example, but much more efficient than the Osher-Solomon Riemann solver [21]. The advantage of our solver is its simplicity and generality. In the next section we apply the k-stage $FORCE^k$ schemes to the Euler equations.

4 Test problems for the Euler equations

To illustrate the performance of one of the methods proposed in this paper we solve the time-dependent one-dimensional non-linear Euler equations for an ideal gas with $\gamma = 1.4$. In all cases we compare the results obtained from the methods presented in this paper with those of the Godunov first-order upwind method used in conjunction with the exact Riemann solver.

4.1 Test 1: a shock tube problem with sonic flow

We solve the Euler equations in the domain $[0, 1]$, subdivided into a left section $[0, 0.3)$ and a right section $[0.3, 1]$. The initial conditions assign data for density, velocity and pressure $\rho_L = 1.0$, $u_L = 3/4$, $p_L = 1.0$ in the left section and $\rho_R = 1/8$, $u_R = 0.0$, $p_R = 0.1$ in the right section. We apply transmissive boundary condition at both ends. The solution includes a right shock, a right contact discontinuity and a left transonic, or sonic rarefaction. The sonic point causes difficulties to numerical methods, particularly those based on linearised Riemann solvers, for which an explicit *entropy fix* must be built into the scheme to avoid the computation of *rarefaction shocks*. Here we solve the problem using $M = 100$ cells and a CFL number of 0.9. Figs. 6 to 9 show results obtained from the 4-stage $FORCE^4$ scheme, shown by symbols; the exact solution is shown by the full line. Figs. 10 to 13 show a comparison between the $FORCE^4$ scheme (full line) and the Godunov scheme (dashed line) used in conjunction with the exact Riemann solver. The exact solution (full line) is also shown. The $FORCE^4$ scheme gives noticeable better results than the Godunov scheme. This is particularly the case for the rarefaction wave, especially near the sonic point. To see the effect of increasing the number of stages in the predictor step, while keeping the mesh size constant (100), in Figs. 14 to 17 we show the results for $FORCE^k$, with $k = 1, 2, 3, 4$, as compared with the exact solution (full line). The plots clearly show that as the number of stages in the predictor step increases (with fixed mesh), we approach the reference solution provided by the Godunov scheme. The 3-stage $FORCE^3$ scheme is sufficiently accurate, as compared with the Godunov scheme used in conjunction with the exact Riemann solver, and is probably a scheme that can be used in practice.

4.2 Test 2: a blast wave problem

To assess the robustness, as well as accuracy, of the $FORCE^k$ schemes, we solve the blast wave problem proposed by Woodward and Colella [40]. The domain consists of a tube of unit length with three sections, a left section between 0.0 and 0.1, a middle section between 0.1 and 0.9 and a right section between 0.9 and 1.0. The initial values for density, particle velocity and pressure are $\rho_L = 1.0$, $u_L = 0.0$, $p_L = 1000.0$ in the left section; $\rho_M = 1.0$, $u_M = 0.0$, $p_M = 0.01$ in the middle section and $\rho_R = 1.0$, $u_R = 0.0$, $p_R = 100.0$ in the right section. Reflective boundary conditions are imposed at both ends. The solution of this problem is very complex and involves multiple wave interaction, as time evolves. For a detailed discussion on the solution see [40]. For all methods we used a CFL number of 0.9 and a mesh of 3000 cells. Results for density at the

output time $t = 0.038$ in the interesting section $[\frac{1}{2}, 0.9]$ are shown in Figs. 18 to 23. The solution includes a left contact discontinuity, which is exceeding smeared by all methods, including the Godunov's method with the exact Riemann solver. The second feature from the left is a shock wave, and most methods perform reasonably well for this shock. The first feature from the right is also a shock wave and the second feature from the right is a contact discontinuity, again badly smeared by all methods. Fig. 18 shows a comparison between the Lax-Friedrichs scheme (symbols) and the the reference first-order solution obtained with the Godunov scheme with the exact Riemann solver. It is known that the Lax-Friedrichs scheme is the most diffusive of all stable three-point monotone schemes. An improvement is obtained if the (one-stage) $FORCE^1$ flux is used, as illustrated in Fig. 19; all waves are more sharply resolved. Fig. 20 shows the result from the 2-stage $FORCE^2$ scheme. For the left contact, this scheme agrees perfectly well with the reference solution. This is also the case for the left shock and for the right shock. There is still as difference for the right contact and extrema. Fig. 21 shows the result from the 3-stage $FORCE^3$ scheme. The solution is very close to the reference solution. Fig. 22 shows the result from the 4-stage $FORCE^4$ flux, which agrees very well with the Godunov scheme with the exact Riemann solver. As a matter of fact, the $FORCE^4$ solution is slightly more accurate than the Godunov solution; this was also observed for Test 1. Finally, the situation is summarised in Fig. 23, where it is clearly seen how the multistage $FORCE^k$ scheme *converges* to the optimal first-order solution, as the number of stages is increased, while keeping the mesh fixed. The Lax-Friedrichs solution is also plotted. As for Test 1, the 3-stage $FORCE^3$ scheme is sufficiently accurate and is probably the scheme to be used for practical computations.

5 Concluding remarks

We have presented a multi-stage predictor-corrector approach to obtain an upwind numerical flux for use in finite volume and discontinuous Galerkin finite element methods. The implementations presented here rely on centred fluxes at each stage. It is demonstrated that as the number of stages is increased we attain comparable accuracy to that of the Godunov method used in conjunction with the exact Riemann solver. Our schemes are applicable to any system of conservation laws, regardless of their complexity. The schemes can be appplied to multi-dimensional problems in the setting of finite volume and discontinuous Galerkin finite element methods. High-order extensions are also possible following any of the current approaches, such as TVD methods, ENO/WENO methods, ADER methods and discontinuous Galerkin methods.

Acknowledgements. This work was carried out while the author was an EPSRC senior visiting fellow (Grant GR N09276) at the Isaac Newton Institute for Mathematical Sciences, University of Cambridge, UK, as joint organiser (with P. G. LeFloch and C. M. Dafermos) of the research programme on *Non-linear Hyperbolic Waves in Phase Dynamics and Astrophysics*, Cambridge, January to July 2003. The support provided is gratefully acknowledged.

References

[1] G. Q. Chen and E. F. Toro. Centred schemes for non-linear hyperbolic equations. Technical Report to appear, Isaac Newton Institute for Mathematical Sciences, University of Cambridge, UK, 2003.

[2] B. Cockburn and C. W. Shu. TVB Runge–Kutta Local Projection Discontinuous Galerkin Method for Conservation Laws II: General Framework. *Math. Comput.*, 52(–):411–, 1989.

[3] B. Cockburn and C. W. Shu. The Runge–Kutta Discontinuous Galerkin Method for Conservation Laws. *J. Comput. Phys.*, 141(–):199–, 1998.

[4] R. Courant, E. Isaacson, and M. Rees. On the Solution of Nonlinear Hyperbolic Differential Equations by Finite Differences. *Comm. Pure. Appl. Math.*, 5:243–255, 1952.

[5] Kolgan N. E. Application of the principle of minimum derivatives to the construction of difference schemes for computing discontinuous solutions of gas dynamics (in Russian). Technical Report 6, Uch. Zap. TsaGI, Russia, 1972.

[6] J. Glimm. Solution in the Large for Nonlinear Hyperbolic Systems of Equations. *Comm. Pure. Appl. Math.*, 18:697–715, 1965.

[7] E. Godlewski and P. A. Raviart. *Numerical Approximation of Hyperbolic Systems of Conservation Laws.* Springer, 1996.

[8] S. K. Godunov. Finite Difference Methods for the Computation of Discontinuous Solutions of the Equations of Fluid Dynamics. *Mat. Sb.*, 47:271–306, 1959.

[9] S. K. Godunov, A. V. Zabrodin, and G. P. Prokopov. –. *J. Comp. Math. Phys. USSR 1 (1962)*, pages 1187–, 1962.

[10] A. Harten. High Resolution Schemes for Hyperbolic Conservation Laws. *J. Comput. Phys.*, 49:357–393, 1983.

[11] A. Harten. On a Class of High Resolution Total Variation Stable Finite Difference Schemes. *SIAM J. Numer. Anal.*, 21(1):1–23, 1984.

[12] A. Harten, B. Engquist, S. Osher, and S. R. Chakravarthy. Uniformly High Order Accuracy Essentially Non–oscillatory Schemes III. *J. Comput. Phys.*, 71:231–303, 1987.

[13] A. Harten and S. Osher. Uniformly High–Order Accurate Nonoscillatory Schemes I. *SIAM J. Numer. Anal.*, 24(2):279–309, 1987.

[14] G. S. Jiang and E. Tadmor. Non–oscillatory Central Schemes for Multi–dimensional Hyperbolic Conservation Laws. *SIAM Journal of Scientific Computing*, 19 (6):1892–1917, 1998.

[15] C. B. Laney. *Computational Gasdynamics.* Cambridge University Press, 1998.

[16] P. D. Lax and B. Wendroff. Systems of Conservation Laws. *Comm. Pure Appl. Math.*, 13:217–237, 1960.

[17] R. J. LeVeque. *Numerical Methods for Conservation Laws.* Birkhäuser Verlag, 1992.

[18] D. Levy, G. Puppo, and G. Russo. Central WENO Schemes for Hyperbolic Systems of Conservation Laws. *Mathgematical Modelling and Numerical Analysis*, 33:547–571, 1999.

[19] H. Nessayahu and E. Tadmor. Non–oscillatory Central Differencing for Hyperbolic Conservation Laws. *J. Comput. Phys.*, 87:408–463, 1990.

[20] S. Osher and S. Chakravarthy. Very High Order Accurate TVD Schemes. *IMA Volumes in Mathematics and its Applications*, 2:229–274, 1984.

[21] S. Osher and F. Solomon. Upwind Difference Schemes for Hyperbolic Conservation Laws. *Math. Comp.*, 38,158:339–374, 1982.

[22] P. L. Roe. Approximate Riemann Solvers, Parameter Vectors, and Difference Schemes. *J. Comput. Phys.*, 43:357–372, 1981.

[23] T. Schwartzkopff, Munz C.D, and E. F. Toro. ADER: High-Order Approach for Linear Hyperbolic Systems in 2D. *J. Scientific Computing*, 17:231–240, 2002.

[24] C. Shu and S. Osher. Efficient Implementation of Essentially Non–oscillatory Shock–Capturing Schemes II. *J. Comput. Phys.*, 83:32–78, 1988.

[25] C. W. Shu. Essentially Non–oscillatory and Weighted Non–oscillatory Schemes for Hyperbolic Conservation Laws. Technical Report ICASE Report No. 97–65, NASA, 1997.

[26] C. W. Shu and S. Osher. Efficient Implementation of Essentially Non–oscillatory Shock–Capturing Schemes. *J. Comput. Phys.*, 77:439–471, 1988.

[27] Y. Takakura and E. F. Toro. Arbitrarily Accurate Non-Oscillatory Schemes for a Non-Linear Conservation Law. *J. Computational Fluid Dynamics*, 11:7–18, 2002.

[28] V. A. Titarev and E. F. Toro. ADER: Arbitrary High Order Godunov Approach. *J. Scientific Computing*, 17:609–618, 2002.

[29] E. F. Toro. On Glimm–Related Schemes for Conservation Laws. Technical Report MMU–9602, Department of Mathematics and Physics, Manchester Metropolitan University, UK, 1996.

[30] E. F. Toro. *Riemann Solvers and Numerical Methods for Fluid Dynamics, Second Edition.* Springer–Verlag, 1999.

[31] E. F. Toro and S. J. Billett. Centred TVD Schemes for Hyperbolic Conservation Laws. *IMA J. Numerical Analysis*, 20:47–79, 2000.

[32] E. F. Toro, R. C. Millington, and L. A. M. Nejad. Towards Very High–Order Godunov Schemes. In *Godunov Methods: Theory and Applications. Edited Review, E. F. Toro (Editor)*, pages 905–937. Kluwer Academic/Plenum Publishers, 2001.

[33] E. F. Toro, M. Spruce, and W. Speares. Restoration of the Contact Surface in the HLL–Riemann Solver. *Shock Waves*, 4:25–34, 1994.

[34] E. F. Toro and V. A. Titarev. Solution of the Generalised Riemann Problem for Advection-Reaction Equations. *Proc. Roy. Soc. London*, 458:128–143, 2002.

[35] E. F. Toro and V. A. Titarev. TVD Fluxes for High-Order ADER Schemes. Technical Report NI03011-NPA, Isaac Newton Institute for Mathematical Sciences, University of Cambridge, UK, 2003.

[36] E. F. (Editor) Toro. *Godunov Methods: Theory and Applications. Edited Review, E. F. Toro (Editor).* Kluwer Academic/Plenum Publishers, 2001.

[37] J. J. W. van der Vegt, van der Ven H., and O. J. Boelens. Discontinuous Galerkin Methods for Partial Differential Equations. In *Godunov Methods: Theory and Applications (Edited Review), E. F. Toro (Editor).* Kluwer Academic/Plenum Publishers, 2001.

[38] B. van Leer. Towards the Ultimate Conservative Difference Scheme I. The Quest for Monotonicity. *Lecture Notes in Physics*, 18:163–168, 1973.

[39] B. van Leer. Towards the Ultimate Conservative Difference Scheme II. Monotonicity and Conservation Combined in a Second Order Scheme. *J. Comput. Phys.*, 14:361–370, 1974.

[40] P. Woodward and P. Colella. The Numerical Simulation of Two–Dimensional Fluid Flow with Strong Shocks. *J. Comput. Phys.*, 54:115–173, 1984.

[41] H. C. Yee. Construction of Explicit and Implicit Symmetric TVD Schemes and their Applications. *J. Comput. Phys.*, 68:151–179, 1987.

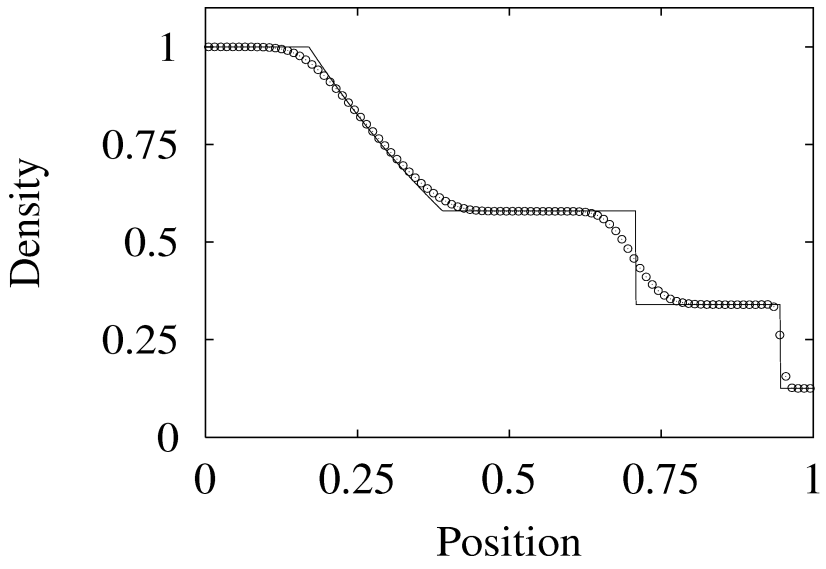

Figure 6: Test 1. Comparison for density between the exact solution (line) and the 4-stage $FORCE^4$ scheme (symbol).

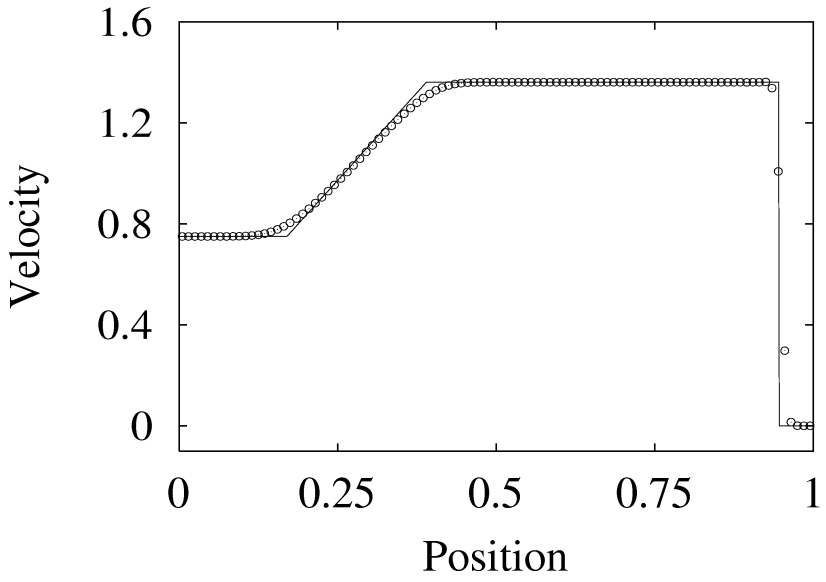

Figure 7: Test 1. Comparison for velocity between the exact solution (line) and the 4-stage $FORCE^4$ scheme (symbol).

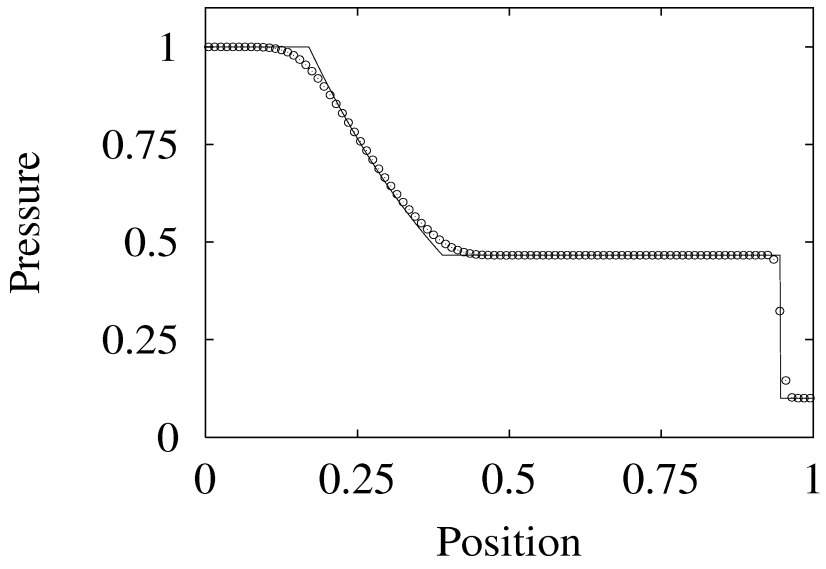

Figure 8: Test 1. Comparison for pressure between the exact solution (line) and the 4-stage $FORCE^4$ scheme (symbol).

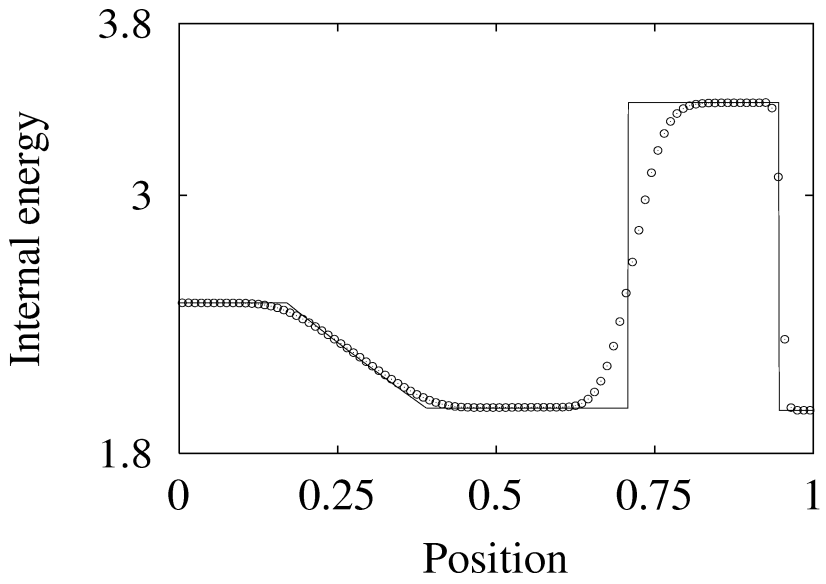

Figure 9: Test 1. Comparison for specific internal energy between the exact solution (line) and the 4-stage $FORCE^4$ scheme (symbol).

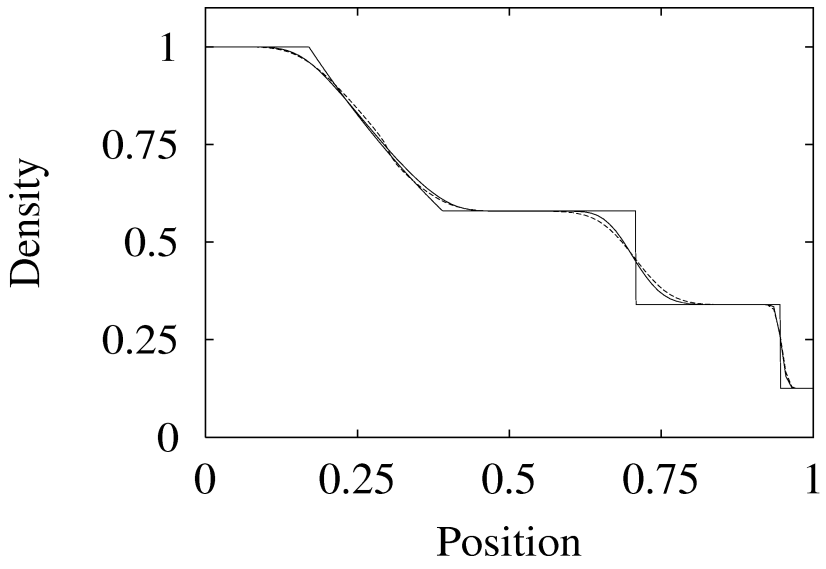

Figure 10: Test 1. Comparison for density between the exact solution (line), the Godunov method (dashed line) and the 4-stage $FORCE^4$ scheme (full line).

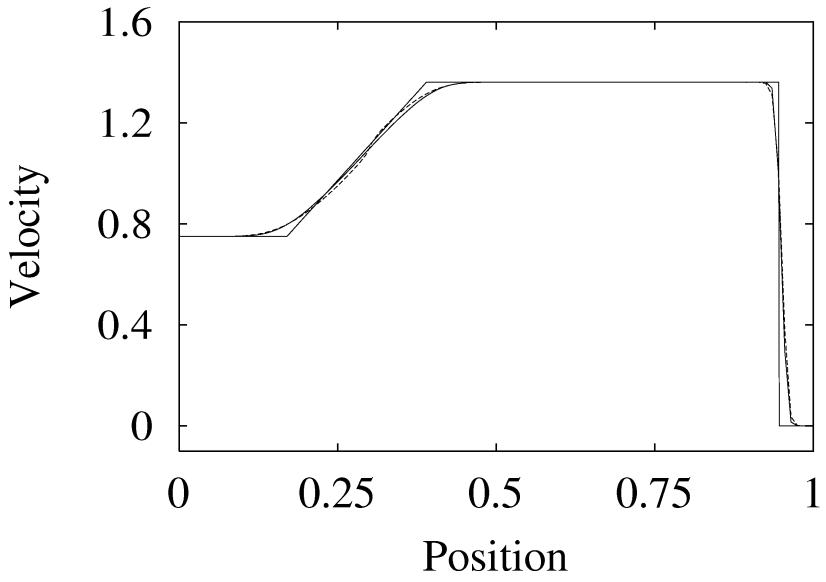

Figure 11: Test 1. Comparison for velocity between the exact solution (line), the Godunov method (dashed line) and the 4-stage $FORCE^4$ scheme (full line).

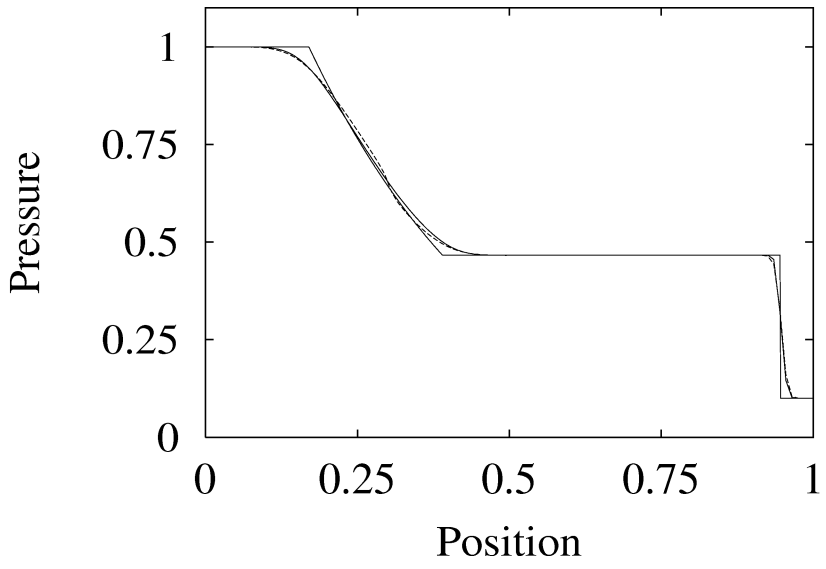

Figure 12: Test 1. Comparison for pressure between the exact solution (line), the Godunov method (dashed line) and the 4-stage $FORCE^4$ scheme (full line).

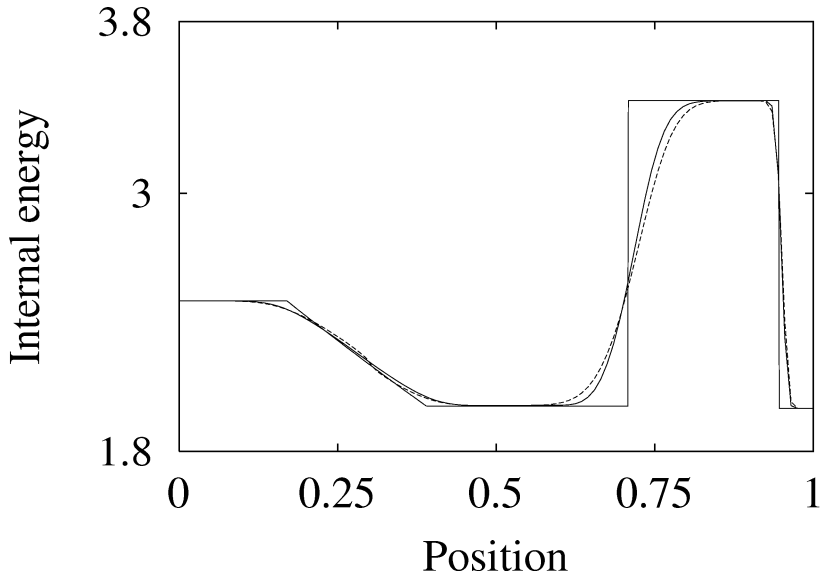

Figure 13: Test 1. Comparison for specific internal energy between the exact solution (line), the Godunov method (dashed line) and the 4-stage $FORCE^4$ scheme (full line).

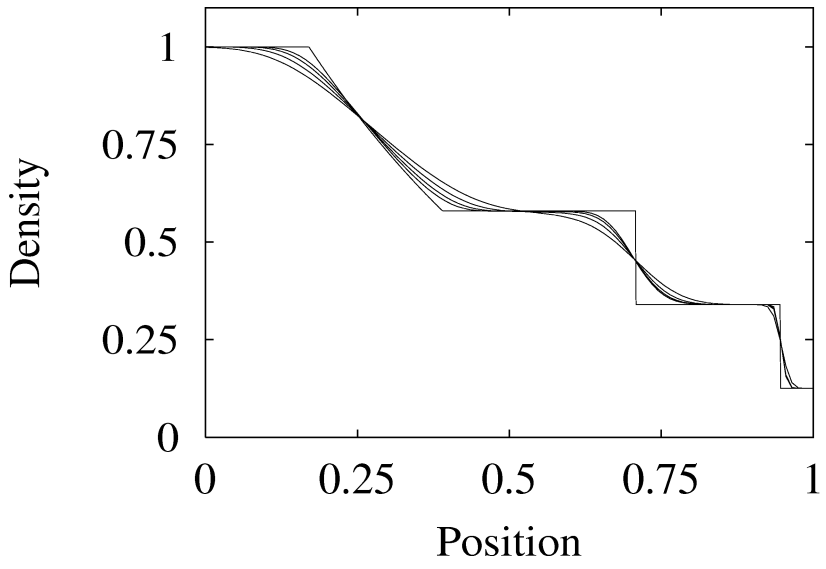

Figure 14: Test 1. Comparison for density between the exact solution (line) and the $FORCE^k$ schemes, $k = 1, 2, 3, 4$ (lines).

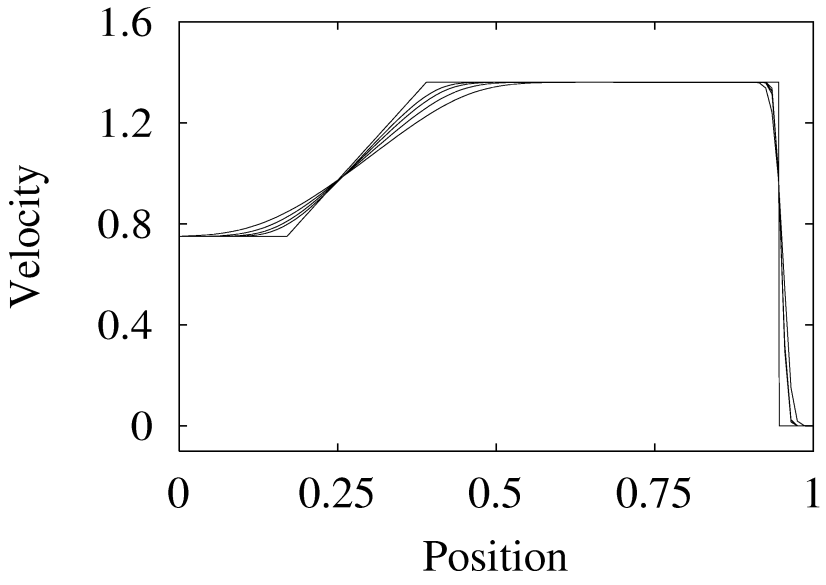

Figure 15: Test 1. Comparison for velocity between the exact solution (line) and the $FORCE^k$ schemes, $k = 1, 2, 3, 4$ (lines).

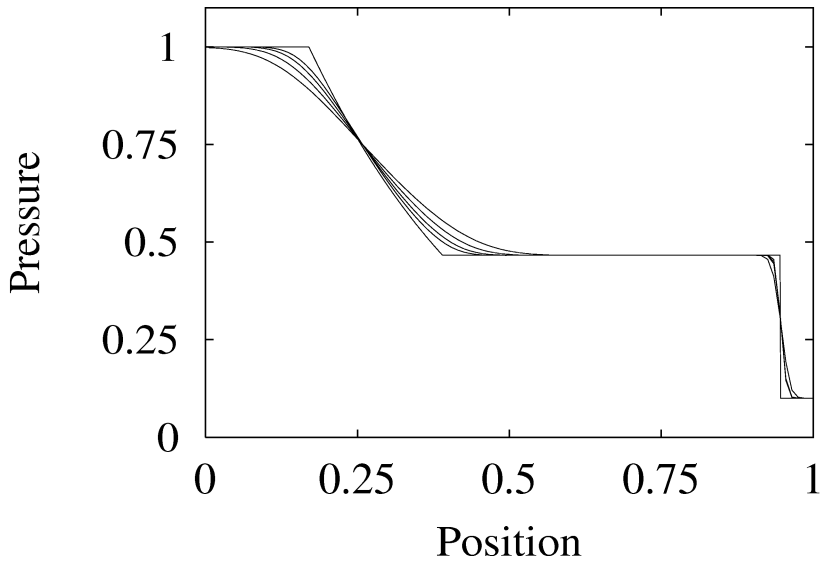

Figure 16: Test 1. Comparison for pressure between the exact solution (line) and the $FORCE^k$ schemes, $k = 1, 2, 3, 4$ (lines).

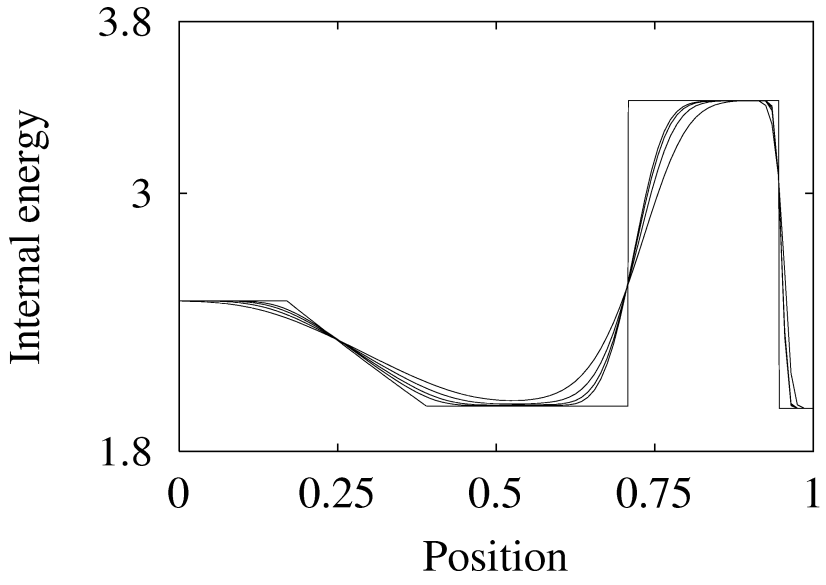

Figure 17: Test 1. Comparison for specific internal energy between the exact solution (line) and the $FORCE^k$ schemes, $k = 1, 2, 3, 4$ (lines).

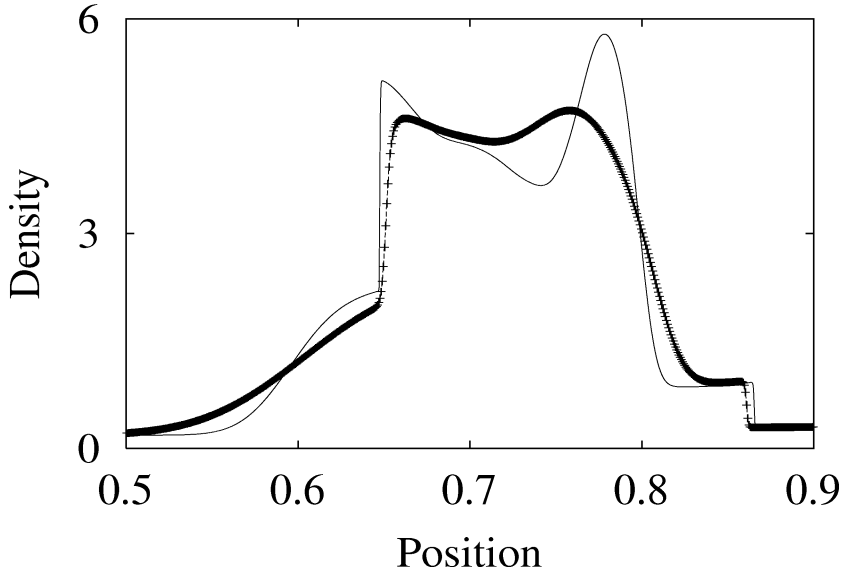

Figure 18: Comparison between the Godunov method (full line) and the Lax-Friedrichs scheme (symbols).

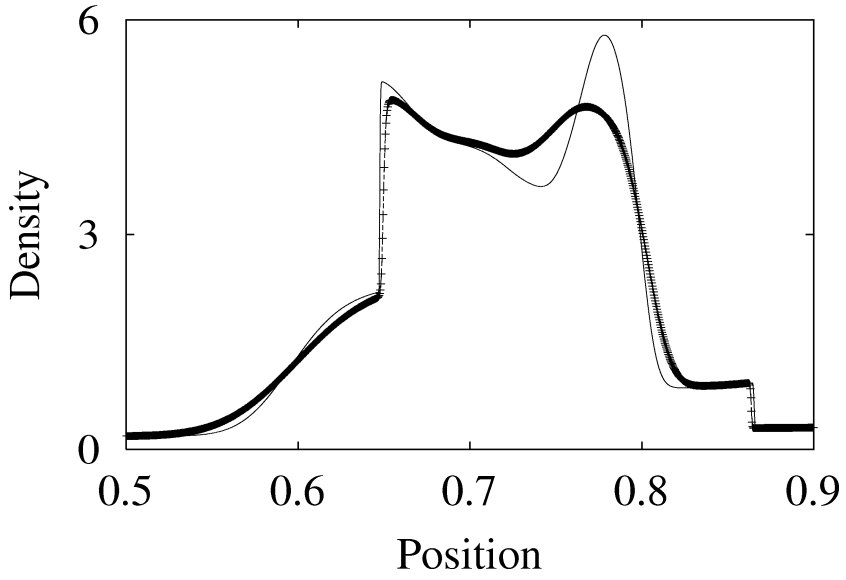

Figure 19: Comparison between the Godunov method (full line) and the FORCE scheme (symbols).

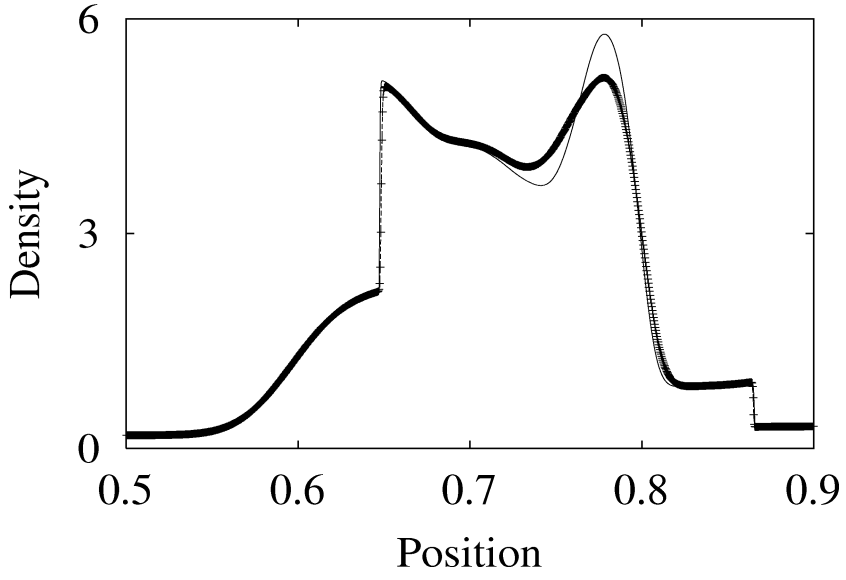

Figure 20: Comparison between the Godunov method (full line) and the 2-stage $FORCE^2$ scheme (symbols).

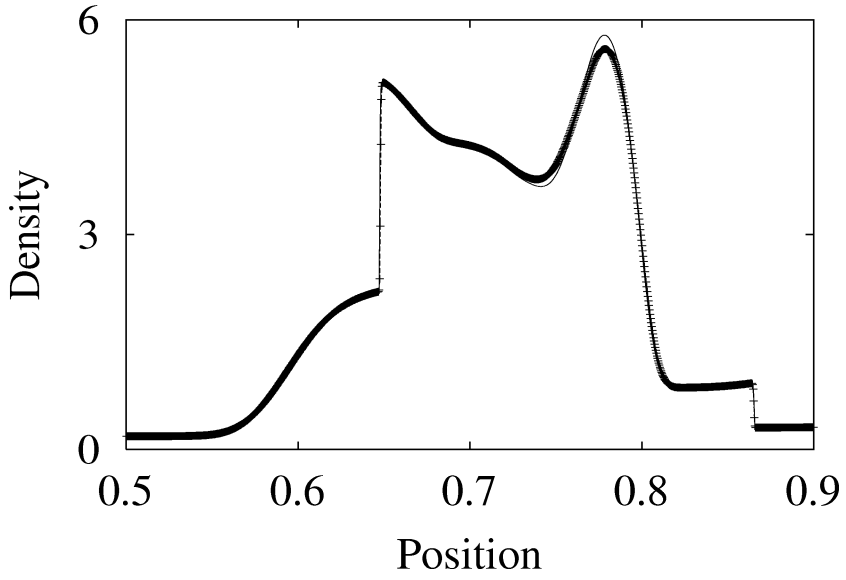

Figure 21: Comparison between the Godunov method (full line) and the 3-stage $FORCE^3$ scheme (symbols).

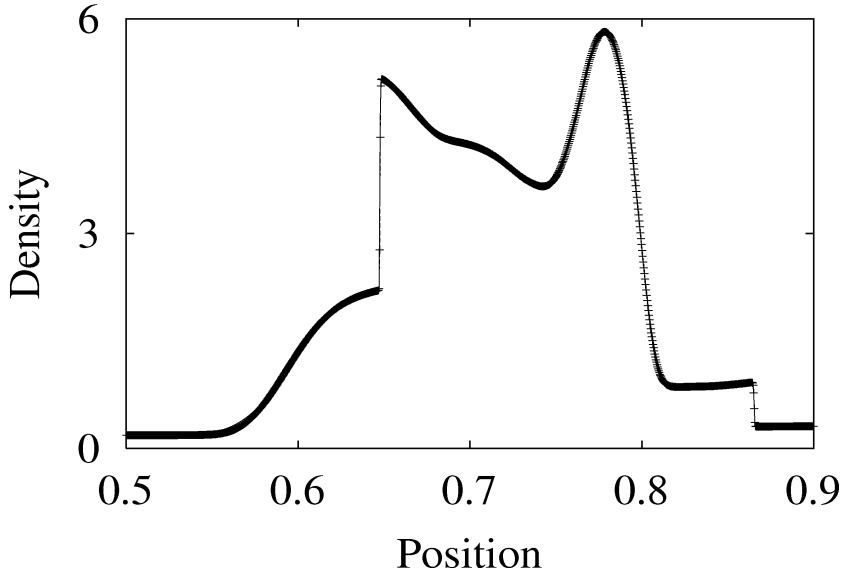

Figure 22: Comparison between the Godunov method (full line) and the 4-stage $FORCE^4$ scheme (symbols).

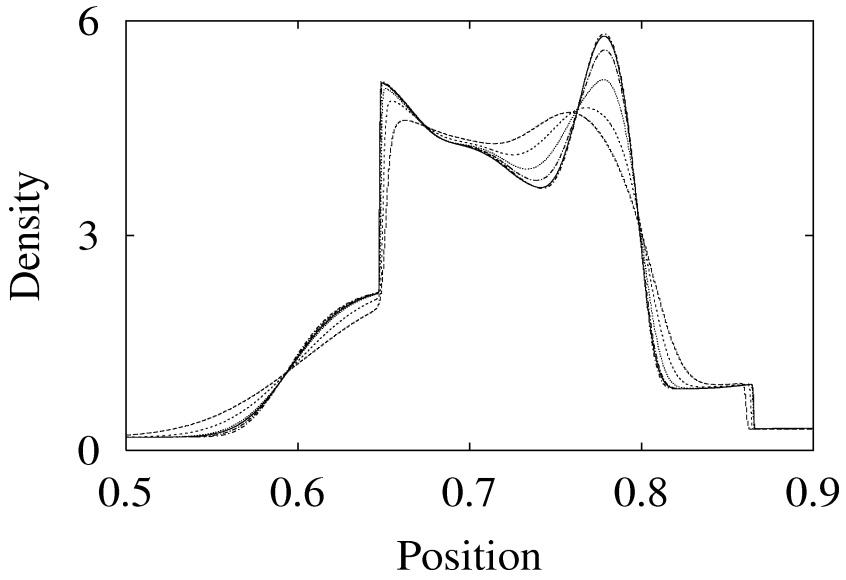

Figure 23: Comparison between the Godunov method and other schemes: Lax-Friedrichs, k-stage $FORCE^k$, for $k = 1, 2, 3, 4$.